Epitaxial Growth and Dielectric Characterization of Atomically Smooth $0.5Ba(Zr_{0.2}Ti_{0.8})O_3–0.5(Ba_{0.7}Ca_{0.3})TiO_3$ Thin Films

Running title: Epitaxial Growth and Dielectric Characterization of Atomically Smooth $0.5Ba(Zr_{0.2}Ti_{0.8})O_3–0.5(Ba_{0.7}Ca_{0.3})TiO_3$ Thin Films

Running Authors: Liu *et al.*

Yang Liu

Mork Family Department of Chemical Engineering and Material Science, University of Southern California, Los Angeles, CA 90089

Zheng Wang

School of Electrical and Computer Engineering, Georgia Institute of Technology, Atlanta, GA 30332

Arashdeep Singh Thind

Institute of Materials Science & Engineering, Washington University in St. Louis, St. Louis, MO 63130

Thomas Orvis

Mork Family Department of Chemical Engineering and Material Science, University of Southern California, Los Angeles, CA 90089

Debarghya Sarkar and Rehan Kapadia

Ming Hsieh Department of Electrical Engineering, University of Southern California, Los Angeles, CA 90089

Albina Y. Borisevich

Center for Nanophase Materials Sciences, Oak Ridge National Laboratory, Oak Ridge, TN 37831

Rohan Mishra

Department of Mechanical Engineering & Materials Science, Washington University in St. Louis, St. Louis, MO 63130

Institute of Materials Science & Engineering, Washington University in St. Louis, St. Louis, MO 63130

Asif Islam Khan

School of Electrical and Computer Engineering, Georgia Institute of Technology, Atlanta, GA 30332

Jayakanth Ravichandran[a)]

Mork Family Department of Chemical Engineering and Material Science, University of Southern California, Los Angeles, CA 90089

Ming Hsieh Department of Electrical Engineering, University of Southern California, Los Angeles, CA 90089

We report the epitaxial growth and the dielectric properties of relaxor ferroelectric $0.5Ba(Zr_{0.2}Ti_{0.8})O_3$–$0.5(Ba_{0.7}Ca_{0.3})TiO_3$ thin films with atomically flat surface on $GdScO_3$ single crystal substrates. We studied the effects of growth conditions, such as substrate temperature and oxygen pressure on the structure of the thin films, as measured by X-ray diffraction, to identify the optimal growth conditions. We achieved sustained layer-by-layer growth of $0.5Ba(Zr_{0.2}Ti_{0.8})O_3$–$0.5(Ba_{0.7}Ca_{0.3})TiO_3$ films as monitored by *in situ* and real time reflective high energy electron diffraction. Atomic force microscopy investigations showed atomically smooth step terrace structures. Aberration-corrected scanning transmission electron microscopy images show good epitaxial relation of the film and the substrate without any line defects. High dielectric constant (~1400) and slim hysteresis loops in polarization-electric field characteristics were observed in $0.5Ba(Zr_{0.2}Ti_{0.8})O_3$–$0.5(Ba_{0.7}Ca_{0.3})TiO_3$ films, which are characteristic of relaxor-type ferroelectric materials.

I. Introduction

Ferroelectric thin films have attracted attention for nonvolatile memories, actuators, transducers, and electro-optic devices. Large ferroelectric, piezoelectric and electro-optic properties are characteristic of complex oxides with perovskite structures such as $PbTiO_3$, $LiNbO_3$, $BaTiO_3$.[1–4] Recent investigations on solid solutions of $BaTiO_3$, specifically $0.5\ Ba(Zr_{0.2}Ti_{0.8})O_3$ – $0.5\ (Ba_{0.7}Ca_{0.3})TiO_3$ (BCZT-50) – a composition near the morphotropic phase boundary,[5] have shown high dielectric constant of 2800, piezoelectric coefficient d_{33} of 500 pC/N and high effective electro-optic coefficient r_c of 530 pm/V.[6–10] With the growing need for on-chip, lossless conversion of electrical to optical signals, especially for visible light, electro-optic modulation is widely explored as a viable solution. For electro-optic applications, one would use the electro-optic oxides as optical waveguides that can act as light modulators. Hence, epitaxial ferroelectric

films with low propagation loss, and large electro-optic coefficients are critical for achieving on-chip modulators.[11]

Synthesis of BCZT thin films have been explored by a variety of methods such as sputtering, chemical solution deposition, screen printing and pulsed laser deposition.[12–16] However, few reports have investigated the epitaxial growth of BCZT thin films. Among the epitaxial growth methods for such ferroelectric alloy thin films, pulsed laser deposition remains one of the facile and reliable approaches. As the performance of non-linear optical materials are often determined by the defects, it is necessary to carefully study the processing-defect relationships for enabling high performance electro-optic modulator.[17] Past studies have explored the effect of growth conditions and thickness on the structure of BCZT thin films on platinized silicon or $SrTiO_3$ substrates.[18–20] Nevertheless, the large mismatch or lack of epitaxial matching has hindered the growth of high quality BCZT films.

Early studies of optical loss on thin film ferroelectric waveguides indicated that scattering by surfaces was the major loss mechanism.[21] Optical losses by scattering and absorption should be low (less than 1 dB/cm) for most applications. A root mean square (rms) roughness of 1 nm can lead to significant scattering of 3 dB/cm.[22] Thus, surface and interface smoothness at the atomic level is critical for low loss operation of electro-optic thin films. Nevertheless, the as-deposited films often display appreciable surface roughness mainly due to a large lattice mismatch of the films and substrates, and the uncontrolled domain structure. To overcome these issues, we selected $GdScO_3$ as a substrate achieve epitaxial thin films of BCZT with low lattice mismatch. The lattice mismatch $m = (d_{film} - d_{substrate})/d_{substrate}$ between orthorhombic $GdScO_3$ ($a_{pseudo\text{-}cubic}$=3.968 Å at 300 K) and tetragonal BCZT-50 (a=4.003 Å, c=4.021 Å at 300 K) is as small as 0.9%.[8]

In this letter, we report the growth of atomically smooth BCZT-50 thin films on (110) $GdScO_3$ substrate. We used a conductive $SrRuO_3$ layer as a bottom electrode to screen the surface charges induced by the polarizations in the BCZT films.[23] We carried out systematic studies by varying the substrate temperature and oxygen partial pressure to understand their effects on the structure of BCZT-50 films and achieve the optimal conditions for high quality films. We performed *in situ* structural analyses using reflection high energy electron diffraction (RHEED), and *ex situ* studies using atomic force microscopy (AFM), high-resolution X-ray diffraction (XRD), and scanning transmission electron microscopy (STEM) to study the surface topography and crystal structure of the films. Finally, we studied the ferroelectric properties of BCZT-50 thin films in the out-of-plane geometry.

II. Method

The BCZT-50 films were prepared by pulsed laser deposition method using a 248 nm KrF excimer laser. We carried out the growth using a dense, polycrystalline ceramic target of BCZT-50 prepared by solid state reaction. $GdScO_3$ (110) single crystal substrates were pre-annealed in an atmosphere of high purity oxygen at 1100°C for 3 hours and then cleaned sequentially in acetone, and isopropanol alcohol prior to the deposition. The chamber was evacuated to a base pressure of 10^{-7} Torr before the introduction of high-purity oxygen. The growth was preceded by a pre-ablation of the target with 500 laser pulses under the deposition pressure. The laser fluence for the growth was fixed at 1.5 J/cm^2 for all the studies reported here. First, a thin layer of $SrRuO_3$ was deposited on $GdScO_3$ substrate to serve as a bottom electrode at the same deposition temperature and oxygen pressure used for BCZT-50. The BCZT-50 films were subsequently deposited on $SrRuO_3$ coated $GdScO_3$ from a dense, polycrystalline, stoichiometric BCZT-50 target

at various substrate temperatures of 650 - 850°C and oxygen pressures of 1 - 50 mTorr. After the deposition, the thin films were slowly cooled to room temperature at a rate of 2°C/min.

The growth rate and thickness of the films were determined *in situ* by RHEED. The lattice parameters of the films were characterized by high-resolution X-ray diffraction (HRXRD) and reciprocal space map (RSM) with Cu K_α radiation. (λ=0.154 nm) The surface topography was investigated using atomic force microscopy (AFM) in the non-contact mode. STEM experiments were carried out using the aberration-corrected Nion UltraSTEM^{TM}200 (operating at 200 kV) microscope at Oak Ridge National Laboratory, which is equipped with a fifth-order aberration corrector and a cold field emission electron gun. Circular electrodes of diameter 10 μm, 25 μm, 50 μm, 100 μm and 200 μm were patterned on the BCZT-50 films by photolithography, followed by metal deposition and lift-off. Electron beam evaporated 5 nm Ti and 100 nm Au was used as the electrode metal stack. The polarization versus electric field measurement was performed using an aixACCT TF-3000 Ferroelectric Parameter Analyzer at 1 kHz. The dielectric constant versus electric field measurement was performed using a Keysight E4990A Impedance Analyzer at 1 kHz.

III. Result and Discussion

We used structural properties derived from X-ray diffraction measurements as the criteria for the optimization of the growth parameters for BCZT-50 thin films. We varied the substrate temperature and the oxygen partial pressure to identify the optimized parameters. First, we varied the substrate temperature, T_s from 650 to 850°C with fixed oxygen partial pressure at 10 mTorr. Fig. 1 (a) shows the XRD plot of ~100nm BCZT-50 films deposited at T_s = 650, 750, 800, and 850°C. The BCZT-50 films exhibit a strong *c*-axis oriented texture with the [110] substrate

crystallographic direction for all temperatures. It is worth noting that we observed thickness fringes around primary reflection in the XRD curve of 750°C. This indicates that the surface of the samples grown at this condition tends to be smooth, also confirmed by AFM in Fig. 4 (c). We observed a gradual shift in the position of reflections for BCZT-50 thin film as a function of the T_s. We show the evolution of the BCZT lattice parameter as a function of the growth temperature in Fig. 1 (b). We observed a clear decrease in the out-of-plane lattice parameter from 4.2 to 4.06 Å as T_s increased from 650 to 850°C. This change in the lattice parameter is ascribed to the relaxation of the strain induced by lattice mismatch of the substrate and film. We also performed rocking curve measurements to study the perfection of the out-of-plane texture of BCZT-50 002 reflections at different growth temperatures. The full-width at half-maximum (FWHM) values of those rocking curves are plotted against the substrate temperature in Fig. 1 (c). The best FWHM value is 0.036° obtained at T_s = 750°C, indicating good crystallinity with excellent out-of-plane texture of the as-grown BCZT-50 films.

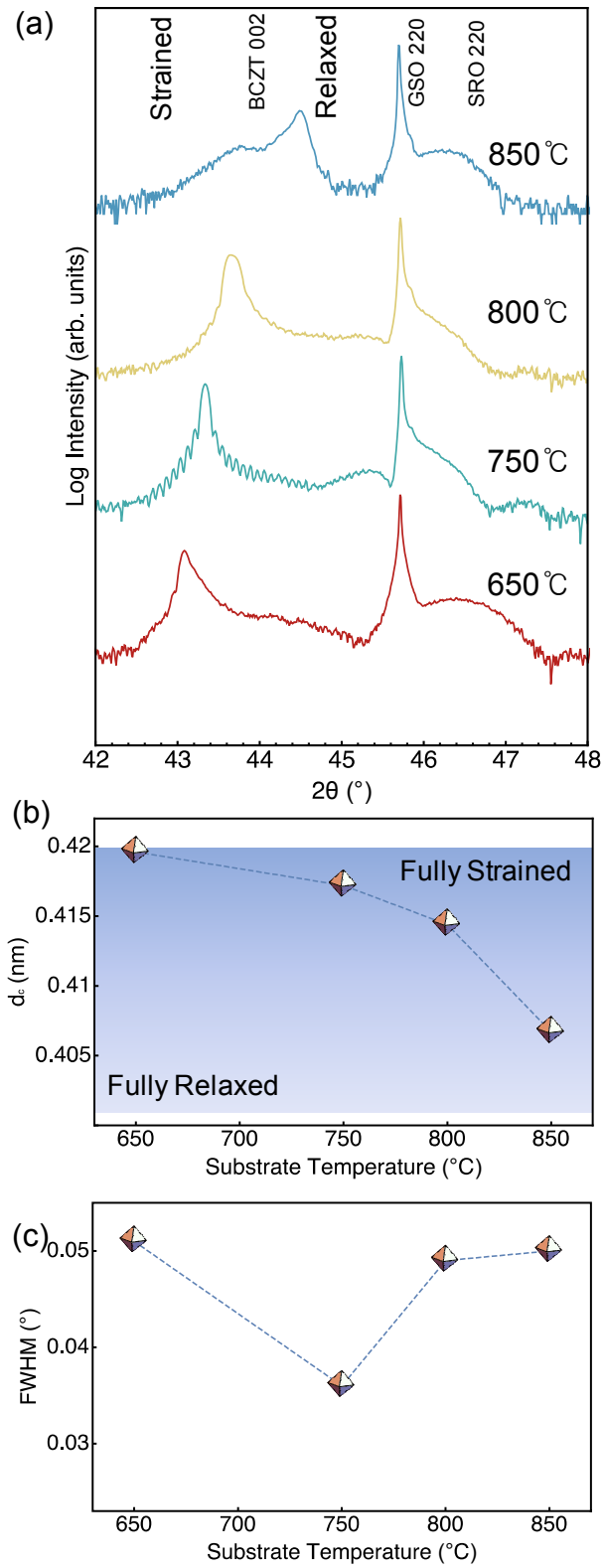

Figure 1. (color online) (a) High resolution, short angular-range XRD plot of BCZT-50 film grown at 650, 750, 800, and 850°C. The dashed lines indicate the position of fully strained and relaxed BCZT-50, $GdScO_3$ (GSO) 220, and $SrRuO_3$ (SRO) 220 reflections. (b) Variation of out of plane lattice spacing of the BCZT-50 thin film with the deposition temperature. (c) Evolution of the full width at half maximum values of rocking curve with the deposition temperature.

The oxygen partial pressure was varied from 1 to 50 mTorr with T_s fixed at 750°C to investigate the effects of oxygen pressure on BCZT-50 films structure. XRD spectra of BCZT-50

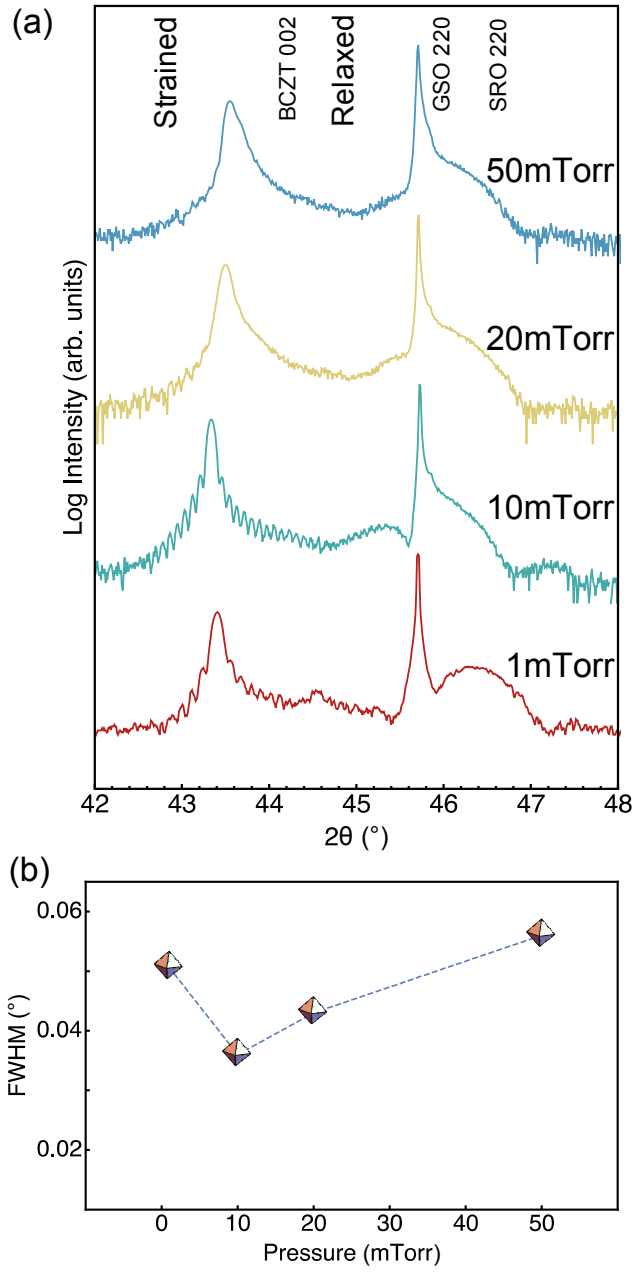

Figure 2. (color online) (a) Out of plane XRD plot of BCZT-50 film grown at 1, 10, 20, and 50 mTorr of oxygen pressure. The dash lines indicate the position of fully strained and relaxed BCZT-50, $GdScO_3$ (GSO) 220, and $SrRuO_3$ (SRO) 220 reflections. (b) The variation of full-width at half-maximum values of rocking curve with the oxygen partial pressure in the deposition chamber.

films grown at 1, 10, 20, and 50 mTorr are shown in Fig. 2 (a). Unlike the temperature series, oxygen pressure plays a lesser role in determining the relaxation state of the film. Instead, it gives us clear guidance to smooth surface. At lower pressure (1 and 10 mTorr), the presence of Pendellösung fringes in the θ-2θ scans indicate a flat surface whereas the high pressures (20 and 50 mTorr) give relatively rough surface. The rocking curve FWHM values of all samples were summarized in Figure 2 (b). The smallest FWHM value obtains at 10 mTorr as 0.036°.

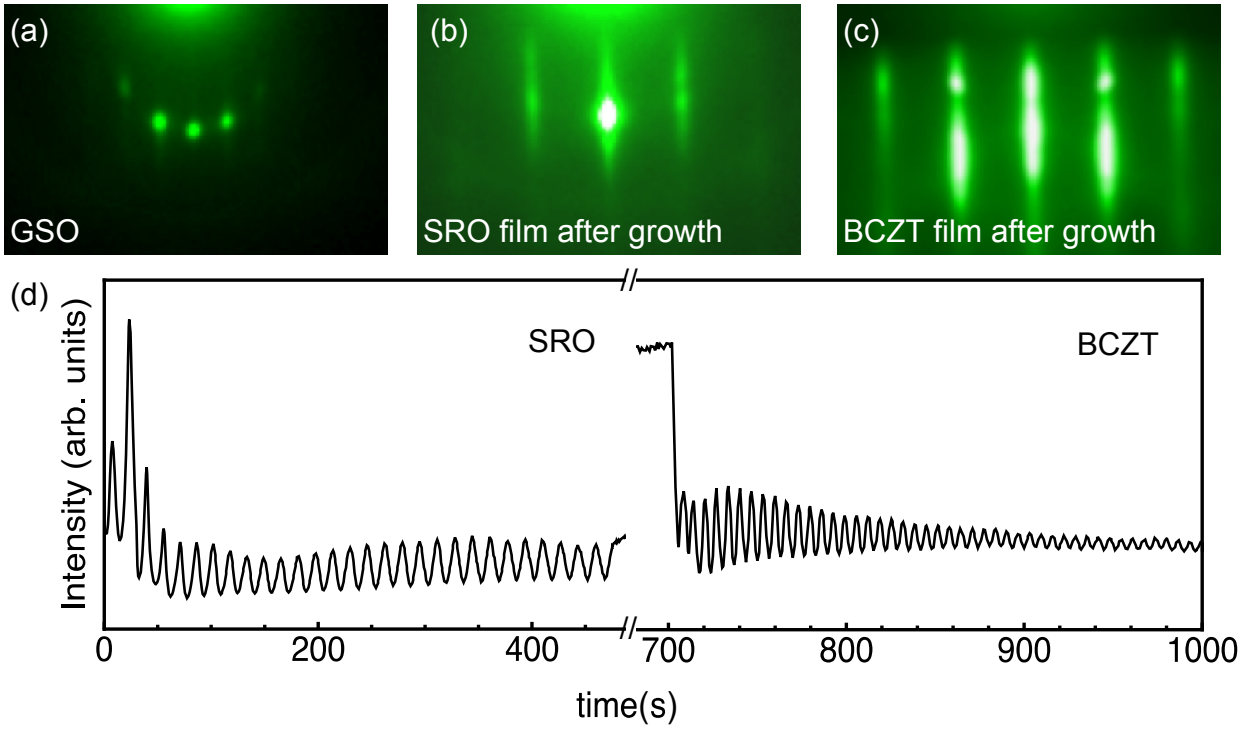

Figure 3. (color online) Representative reflection high energy electron diffraction patterns of : (a) $GdScO_3$ (GSO) substrate, (b) $SrRuO_3$ (SRO) bottom electrode, and (c) BCZT-50 film. (d) Specular spot intensity oscillations of $SrRuO_3$ and BCZT-50 film.

In Fig. 3, we present a set of representative RHEED patterns and intensity oscillations of the specular spot at the optimal condition of 750 °C and 10 mTorr. At first, the annealed $GdScO_3$ substrates exhibited a clear 2D diffraction pattern, which attests to the presence of highly smooth

$GdScO_3$ surface. During the deposition of $SrRuO_3$, well defined diffraction and specular spots with streaky pattern, and RHEED intensity oscillations were observed. We grew 12 nm thick $SrRuO_3$ layer and estimated the growth rate of $SrRuO_3$ to be 0.049 Å/pulse. We followed the $SrRuO_3$ deposition with the growth of BCZT-50. Initially, the 2D diffraction pattern was retained with the subtle change in the diffraction spots corresponding to the larger lattice parameter of BCZT-50. As the growth continued, the diffraction spots gradually transformed to become streaks. The streaky pattern remained till the end of growth, which again indicates a relatively smooth surface. The Fig. 3 (c) shows the RHEED pattern at the end of the growth of a 100 nm thick BCZT-50 film. As an evidence of layer-by-layer growth, we show the oscillations in the intensity of the specular spot for BCZT-50 in Fig. 3 (d). The growth rate of BCZT-50 was estimated as 0.135 Å/pulse. To

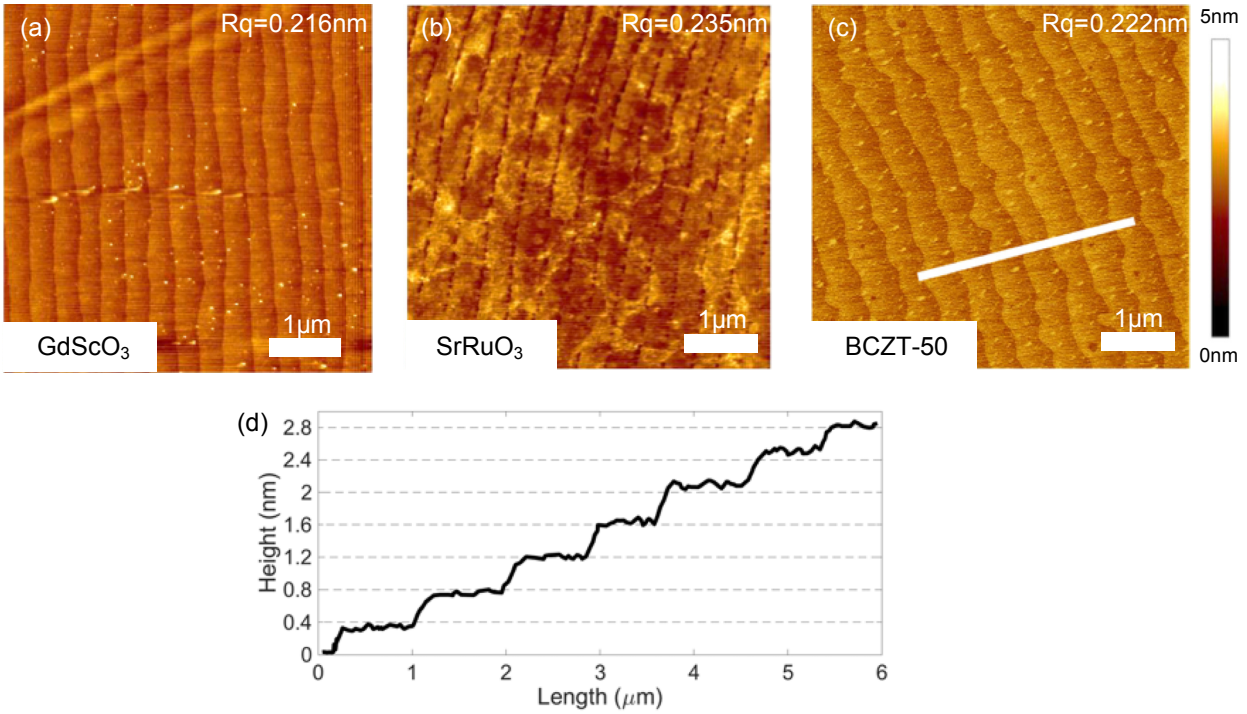

Figure 4. (color online) Representative topography image of (a) annealed $GdScO_3$ substrate, (b) $SrRuO_3$ film, and (c) BCZT-50 film surface. (d) Cross-sectional profile of BCZT-50 film showing the step height. The distance between two horizontal guide lines is 4 Å, which corresponds to the lattice spacing expected in single-layer-step.

quantitatively analyze the interface and surface roughness obtained upon the growth, we preformed AFM studies on three different samples of annealed $GdScO_3$ substrate, 15 nm $SrRuO_3$ on $GdScO_3$ and 100 nm BCZT-50 film on 15 nm $SrRuO_3/GdScO_3$ substrate as shown in Fig 4. Overall, all the surfaces have a root mean square roughness of ~2 Å or less. $SrRuO_3$ has a relatively smooth surface while the step feature is not readily apparent. The annealed substrate and BCZT-50 film exhibit atomically smooth surface with step terraces. The height of the steps corresponds to single unit cell as shown in Fig 4 (d).

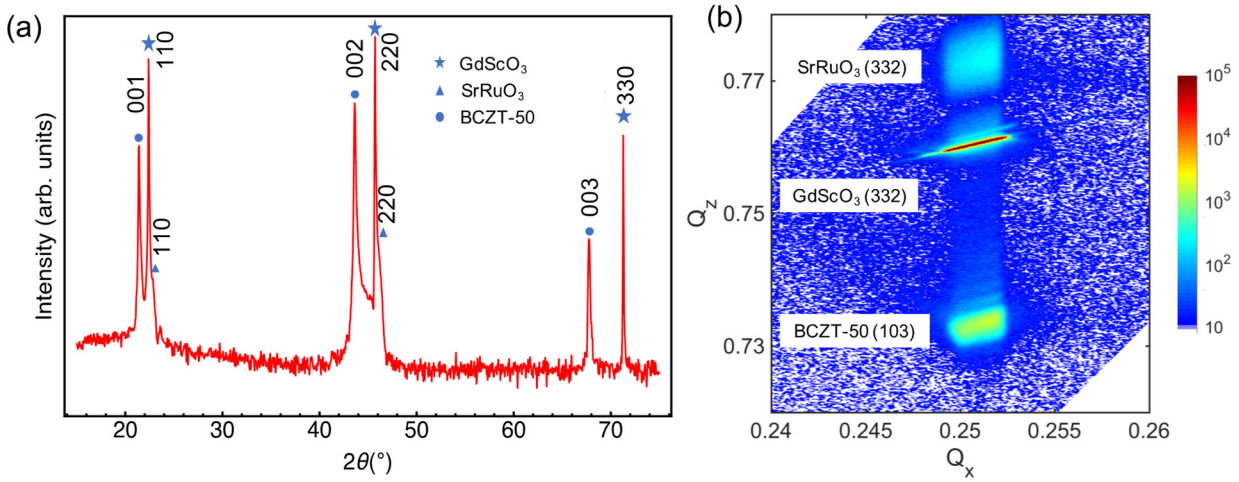

Figure 5. (color online) (a) XRD plot of a representative BCZT-50 thin film. (b) A high-resolution reciprocal space map of BCZT-50 thin film centered on $GdScO_3$ 332 substrate peak. The map clearly shows the film is coherently strained to the substrate.

To establish the epitaxial relationship between the film and the substrate, we performed high-resolution XRD, RSM and STEM studies. Fig 5 (a) shows a representative XRD pattern from a 50 nm BCZT-50 thin film grown at 750 °C and 10 mTorr, where only 00*l* family of reflections are visible for the BCZT-50 thin film with the *ll*0 reflections of the substrate, which correspond the pseudo-cubic 00*l* reflections. This indicates that the BCZT-50 is highly oriented along the out-of-plane direction of $GdScO_3$ substrate. The $SrRuO_3$ layer reflections are not readily observed due

to weak reflections arising from its ultrathin nature, but one could clearly observe them in Figure 1 and 2. To further illustrate the in-plane epitaxial relationships, we performed RSM studies centered on 332 $GdScO_3$ reflection. We observed three reflections corresponding to $SrRuO_3$, $GdScO_3$ and BCZT-50 in the RSM. All of three reflections possess the same in-plane reciprocal lattice parameter (q_x), which indicates all the layers are fully strained to the substrate with negligible relaxation. For the out-of-plane (q_z) direction, the lattice constants agree well with the out-of-plane lattice parameters obtained from 2θ-θ scans. Based on these results, we conclude that BCZT films were epitaxially grown on $GdScO_3$ (110) substrates with the following epitaxial relationship: BCZT(001)||$GdScO_3$(110) and BCZT[100]||$GdScO_3$[001].

To investigate the atomic structure of BCZT/SRO heterostructures, STEM experiments were performed on BCZT (109 nm)/$SrRuO_3$ (15 nm) thin film. Cross-sectional high-angle annular dark-field (HAADF) STEM images clearly revealed that films of BCZT and $SrRuO_3$ were fully strained on the $GdScO_3$ substrate as shown in figure 6 (a). We did not observe any misfit dislocations at the film/substrate interface. The atomic resolution HAADF image in STEM is obtained by elastic scattering of the electron beam from different atomic columns (Ba, Ca, Zr, and Ti), where the degree of elastic scattering is approximately proportional to the squared atomic number ($\sim Z^2$).[24] Therefore, it is easy to distinguish the elements by the brightness of the atomic columns. As a result, atomic columns corresponding to (Ba, Ca) appear brighter than the (Ti, Zr) atomic columns. This is consistent with the theoretical structure of BCZT that is overlaid in Figure 6 (b) with negligible lattice parameter difference.[5,8] Sharp interfaces of between $SrRuO_3$/$GdScO_3$ and BCZT/$SrRuO_3$ were observed and confirmed in figure 6 (b) and (c).

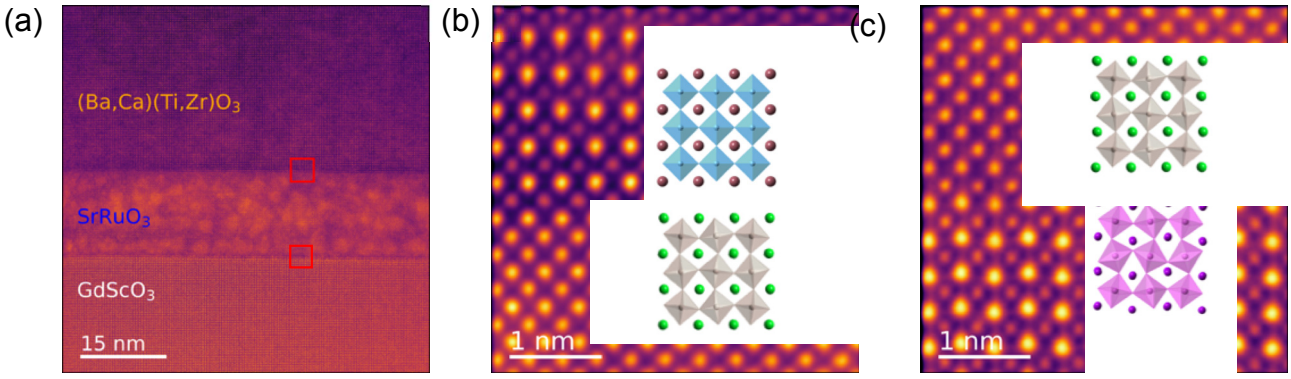

Figure 6. (color online) (a) Cross-sectional low-magnification HAADF image of a BCZT/$SrRuO_3$/$GdScO_3$ sample. No obvious misfit dislocations were observed in BCZT thin film. Atomic resolution HAADF images of (b) BCZT/$SrRuO_3$ and (c) $SrRuO_3$/$GdScO_3$ interfaces with overlaid atomic models. The brown, blue, green, grey, purple, and pink atomic symbols correspond to (Ba, Ca), (Ti, Zr), Sr, Ru, Gd and, Sc elements, respectively.

Figure 7 (a) shows the dielectric constant (ε_r) vs. electric field (E) characteristics of a 200 nm BCZT-50 capacitor with $SrRuO_3$ and Au/Ti electrodes measured at 1 kHz for both upward and downward sweeps. A slight shift in the $\varepsilon_r - E$ characteristics between upward and downward sweeps is observed, and at their intersection, ε_r=1400 is measured. The corresponding phase angle of the impedance spectroscopy is shown in Figure 7 (b). This demonstrates that the sample has low loss with the phase angle close to 90° over the range of applied electric field. Figure 7 (c) depicts the measured polarization (P)-electric field (E) characteristics at f=1 kHz of the same sample. Note in Fig. 7 (c) that the hysteresis in the P-E curve has a narrow opening; such slim hysteresis loops are characteristic of ferroelectric relaxors.[25] Our measured remnant polarization (P_r) of 3.5 $\mu C/cm^2$ and coercive field (E_c) of 26 kV/cm are in the same range of BCZT-50 films as previously reported by Luo et al.[26]

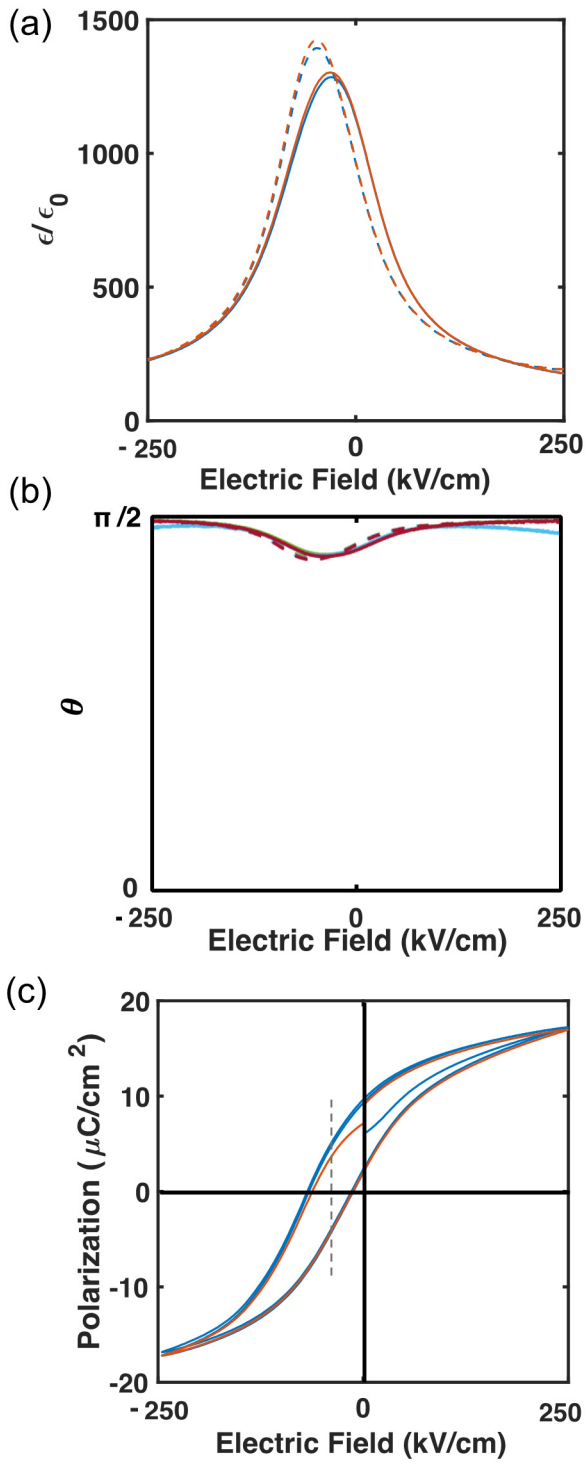

Figure 7. (color online) (a) Dielectric constant and (b) impedance angle as a function of DC electric field at room temperature (solid line and dash line indicate the scans with increasing and decreasing electric fields) and (c) ferroelectric hysteresis loop of a typical BCZT-50 film. Dash line indicates the build-in electric field. The blue and red lines correspond to sweeps starting with positive and negative applied electric fields.

In addition, the P-E hysteresis loop are not symmetric with respect to the origin which is presumably due to our use of different metallic layers with different work functions as top and bottom electrodes (top Au/Ti, bottom: $SrRuO_3$). The resulting built-in electric field is calculated to be -38 kV/cm. This built-in electric field has also been reported in many compositional ferroelectric films, such as $(Ba,Sr)TiO_3$, $Pb(Zr,Ti)O_3$, and BCZT superlattices.[27–29] The origin of the internal field are still not completely understood. Both intrinsic (polarization gradient, free space charge, etc.) and extrinsic (asymmetric contact, strain at interface, oxygen vacancies, etc.)[30] factors could play a role in the offset of the polarization or the built-in electric field.[31,32]

IV. Conclusion

In summary, we have shown high-quality epitaxial growth of BCZT-50 thin films on $SrRuO_3/GdScO_3$ substrates. The growth condition has been optimized based on crystallinity as deduced by XRD studies. Sustained layer-by-layer growth mode was achieved as monitored by RHEED. Atomic force microscopy studies reveal one-unit cell high steps with atomically flat terraces in as-grown BCZT-50 film surfaces. STEM studies did not reveal evidence of misfit dislocations and strain relaxation, confirming high quality interfaces between substrate/$SrRuO_3$ and BCZT/$SrRuO_3$. A relaxor ferroelectric behavior has been observed with relatively high dielectric constant. These studies establish a pathway for further applications in electronic and photonic devices for BCZT thin films.

Acknowledgement

This work was supported by the Air Force Office of Scientific Research under award number FA9550-16-1-0335. We acknowledge the use of Center for Excellence in Nano Imaging for the characterization of the thin films. Z.W. and A.I.K. acknowledge support from the National Science

Foundation (NSF) grant no. 1718671. R. K. acknowledges support from the NSF award no. 1610604. A.S.T. and R.M. acknowledge support from NSF grant no. DMR-1806147.

[1] B. Jaffe, W. Cook, and H. Jaffe, *Piezoelectric Ceramics* (1971).

[2] Z.-G. Ye, *Handbook of Advanced Dielectric, Piezoelectric and Ferroelectric Materials* (Woodhead Publishing Limited, 2008).

[3] R. Weis and T. Gaylord, Appl. Phys. A Mater. Sci. Process. **37**, 191 (1985).

[4] S. Zhang and F. Li, J. Appl. Phys. **111**, 031301 (2012).

[5] A. Bjørnetun Haugen, J.S. Forrester, D. Damjanovic, B. Li, K.J. Bowman, and J.L. Jones, J. Appl. Phys. **113**, 0 (2013).

[6] D. Xue, Y. Zhou, H. Bao, C. Zhou, J. Gao, and X. Ren, J. Appl. Phys. **109**, 054110 (2011).

[7] W. Liu and X. Ren, Phys. Rev. Lett. **103**, 257602 (2009).

[8] D.S. Keeble, F. Benabdallah, P.A. Thomas, M. Maglione, and J. Kreisel, Appl. Phys. Lett. **102**, 092903 (2013).

[9] L. Zhang, M. Zhang, L. Wang, C. Zhou, Z. Zhang, Y. Yao, L. Zhang, D. Xue, X. Lou, and X. Ren, Appl. Phys. Lett. **105**, 162908 (2014).

[10] A.D. Dupuy, Y. Kodera, and J.E. Garay, Adv. Mater. **28**, 7970 (2016).

[11] K. Nashimoto, D.K. Fork, and T.H. Geballe, Appl. Phys. Lett. **60**, 1199 (1992).

[12] K. ichi Mimura, T. Naka, T. Shimura, W. Sakamoto, and T. Yogo, Thin Solid Films **516**, 8408 (2008).

[13] Y. Lin, G. Wu, N. Qin, and D. Bao, Thin Solid Films **520**, 2800 (2012).

[14] W. Bai, B. Shen, F. Fu, and J. Zhai, Mater. Lett. **83**, 20 (2012).

[15] A. Piorra, A. Petraru, H. Kohlstedt, M. Wuttig, and E. Quandt, J. Appl. Phys. **109**, 3 (2011).

[16] W. Li, J. Hao, H. Zeng, and J. Zhai, Curr. Appl. Phys. **13**, 1205 (2013).

[17] M.E. Hagerman and K.R. Poeppelmeier, Chem. Mater. **7**, 602 (1995).

[18] Q. Lin, D. Wang, and S. Li, J. Am. Ceram. Soc. **98**, 2094 (2015).

[19] V. Ion, F. Craciun, N.D. Scarisoreanu, A. Moldovan, A. Andrei, R. Birjega, C. Ghica, F. Di Pietrantonio, D. Cannata, M. Benetti, and M. Dinescu, Sci. Rep. **8**, 2056 (2018).

[20] K. Prabahar, R. Ranjith, A. Srinivas, S.V. Kamat, B. Mallesham, V.L. Niranjani, J.P. Praveen, and D. Das, Ceram. Int. **43**, 5356 (2017).

[21] D.K. Fork, F. Armani-Leplingard, J.J. Kingston, and G.B. Anderson, MRS Proc. **392**, 189 (1995).

[22] L. Beckers, J. Schubert, W. Zander, J. Ziesmann, A. Eckau, P. Leinenbach, and C. Buchal, J. Appl. Phys. **83**, 3305 (1998).

[23] S. Hong, S.M. Nakhmanson, and D.D. Fong, Reports Prog. Phys. **79**, 076501 (2016).

[24] S.J. Pennycook and D.E. Jesson, Ultramicroscopy **37**, 14 (1991).

[25] S. V Kalinin, A.N. Morozovska, and L. Qing, Reports Prog. Phys. **61**, 1267 (1998).

[26] B.C. Luo, D.Y. Wang, M.M. Duan, and S. Li, Appl. Phys. Lett. **103**, 122903 (2013).

[27] V. Romero-Rochín, R.M. Koehl, C.J. Brennan, and K.A. Nelson, J. Chem. Phys. **111**, 3559 (1999).

[28] D. Bao, N. Wakiya, K. Shinozaki, N. Mizutani, and X. Yao, J. Appl. Phys. **90**, 506 (2001).

[29] Q. Lin, D. Wang, Z. Chen, W. Liu, S. Lim, and S. Li, ACS Appl. Mater. Interfaces **7**, 26301 (2015).

[30] Y.-M. Kim, A. Morozovska, E. Eliseev, M.P. Oxley, R. Mishra, S.M. Selbach, T. Grande, S.T. Pantelides, S. V. Kalinin, and A.Y. Borisevich, Nat. Mater. **13**, 1019 (2014).

[31] H.K. Chan, C.H. Lam, and F.G. Shin, J. Appl. Phys. **95**, 2665 (2004).

[32] G. Akcay, S. Zhong, B.S. Allimi, S.P. Alpay, and J. V. Mantese, Appl. Phys. Lett. **91**, 012904

(2007).

Figure Caption List:

Figure 1. (color online) (a) High resolution, short angular-range XRD plot of BCZT-50 film grown at 650, 750, 800, and 850°C. The dashed lines indicate the position of fully strained and relaxed BCZT-50, $GdScO_3$ (GSO) 220, and $SrRuO_3$ (SRO) 220 reflections. (b) Variation of out of plane lattice spacing of the BCZT-50 thin film with the deposition temperature. (c) Evolution of the full width at half maximum values of rocking curve with the deposition temperature.

Figure 2. (color online) (a) Out of plane XRD plot of BCZT-50 film grown at 1, 10, 20, and 50 mTorr of oxygen pressure. The dash lines indicate the position of fully strained and relaxed BCZT-50, $GdScO_3$ (GSO) 220, and $SrRuO_3$ (SRO) 220 reflections. (b) The variation of full-width at half-maximum values of rocking curve with the oxygen partial pressure in the deposition chamber.

Figure 3. (color online) Representative reflection high energy electron diffraction patterns of : (a) $GdScO_3$ (GSO) substrate, (b) $SrRuO_3$ (SRO) bottom electrode, and (c) BCZT-50 film. (d) Specular spot intensity oscillations of $SrRuO_3$ and BCZT-50 film.

Figure 4. (color online) Representative topography image of (a) annealed $GdScO_3$ substrate, (b) $SrRuO_3$ film, and (c) BCZT-50 film surface. (d) Cross-sectional profile of BCZT-50 film showing the step height. The distance between two horizontal guide lines is 4 Å, which corresponds to the lattice spacing expected in single-layer-step.

Figure 5. (color online) (a) XRD plot of a representative BCZT-50 thin film. (b) A high-resolution reciprocal space map of BCZT-50 thin film centered on $GdScO_3$ 332 substrate peak. The map clearly shows the film is coherently strained to the substrate.

Figure 6. (color online) (a) Cross-sectional low-magnification HAADF image of a BCZT/$SrRuO_3$/$GdScO_3$ sample. No obvious misfit dislocations were observed in BCZT thin film. Atomic resolution HAADF images of (b) BCZT/$SrRuO_3$ and (c) $SrRuO_3$/$GdScO_3$ interfaces with overlaid atomic models. The brown, blue, green, grey, purple, and pink atomic symbols correspond to (Ba, Ca), (Ti, Zr), Sr, Ru, Gd and, Sc elements, respectively.

Figure 7. (color online) (a) Dielectric constant and (b) impedance angle as a function of DC electric field at room temperature (solid line and dash line indicate the upward and downward scan of the electric field,) and (c) ferroelectric hysteresis loop of a typical BCZT-50 film. Dash line indicates the build-in electric field. The blue and red lines correspond to sweeps starting from positive and negative direction.

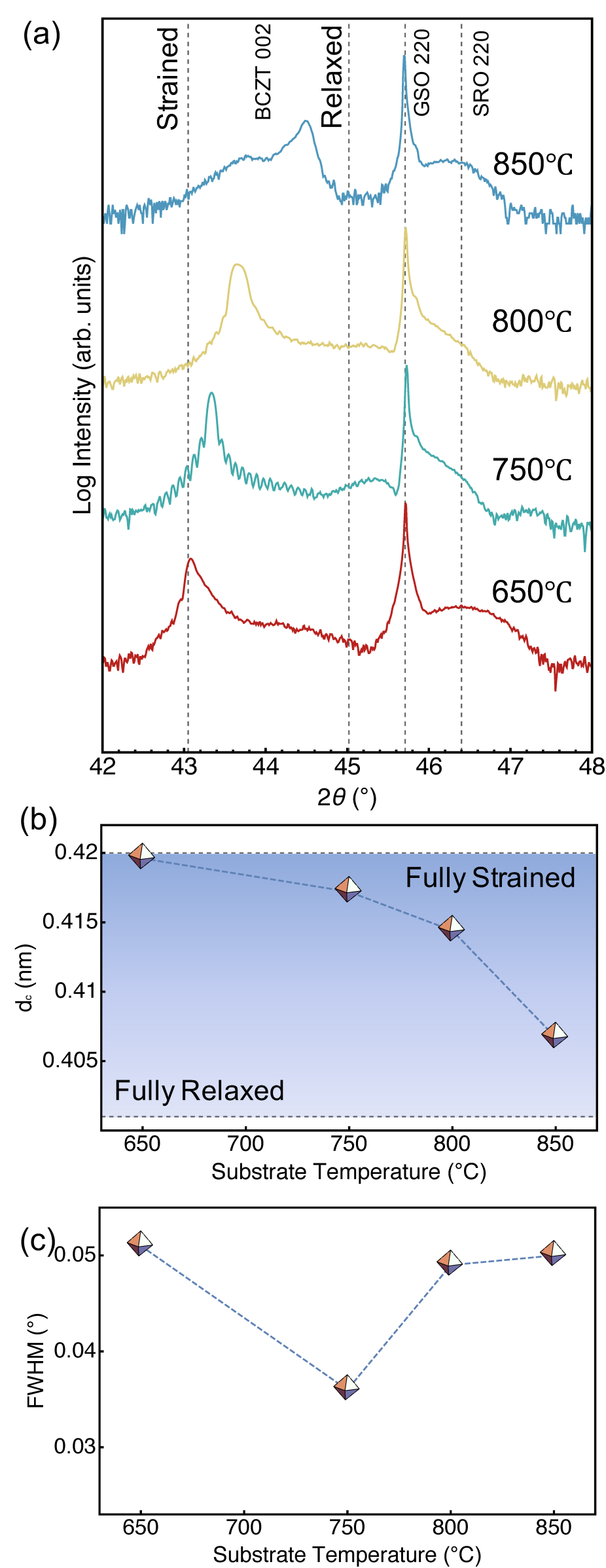
(a)
Strained
BCZT 002
Relaxed
GSO 220
SRO 220
850℃
800℃
750℃
650℃
Log Intensity (arb. units)
42
43
44
45
46
47
48
2θ (°)
(b)
0.42
0.415
0.41
0.405
dc (nm)
Fully Strained
Fully Relaxed
650
700
750
800
850
Substrate Temperature (°C)
(c)
0.05
0.04
0.03
FWHM (°)
650
700
750
800
850
Substrate Temperature (°C)

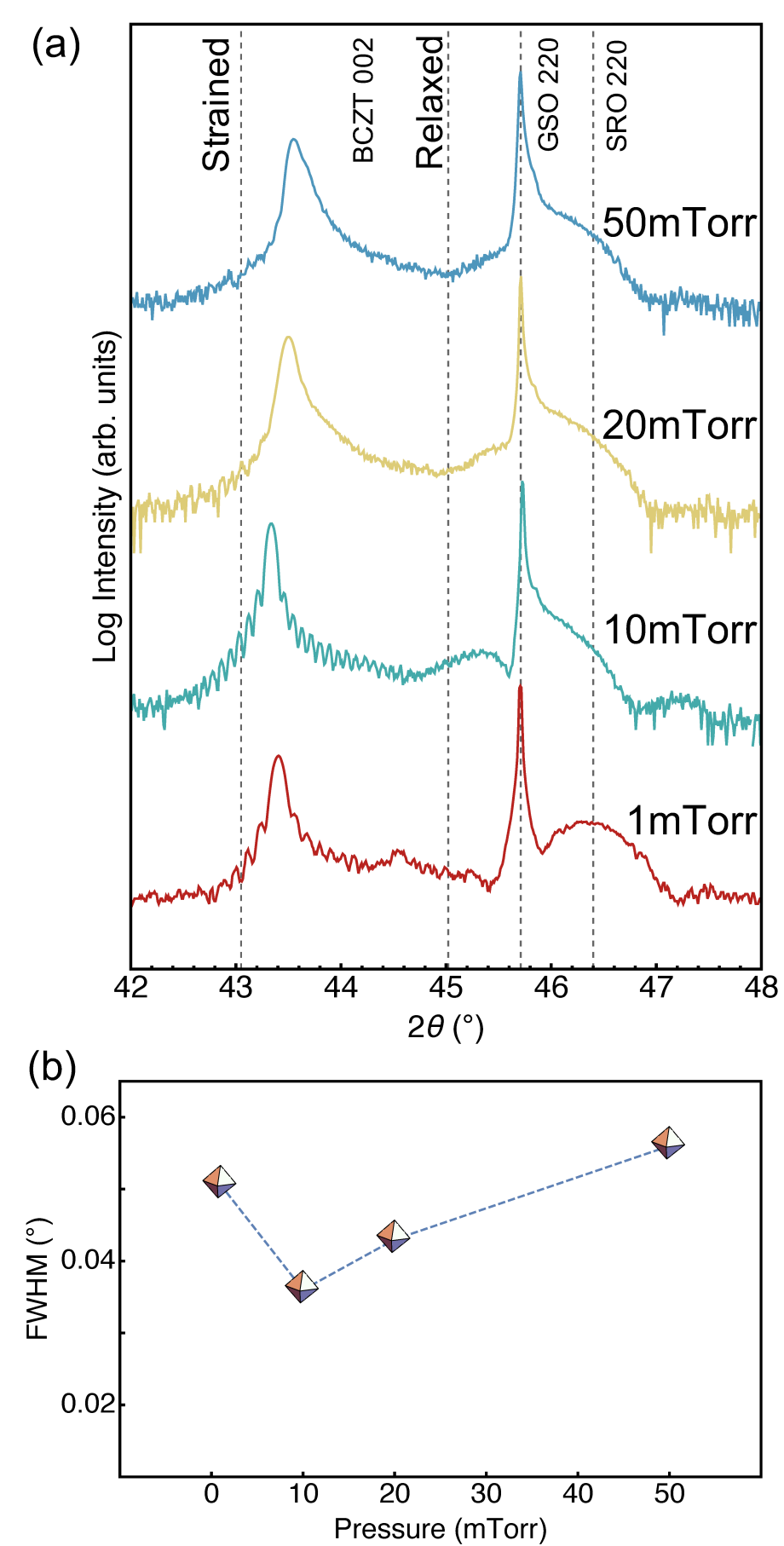
(a)
Strained
BCZT 002
Relaxed
GSO 220
SRO 220
50mTorr
20mTorr
10mTorr
1mTorr
Log Intensity (arb. units)
42
43
44
45
46
47
48
2θ (°)
(b)
0.06
0.04
0.02
FWHM (°)
0
10
20
30
40
50
Pressure (mTorr)

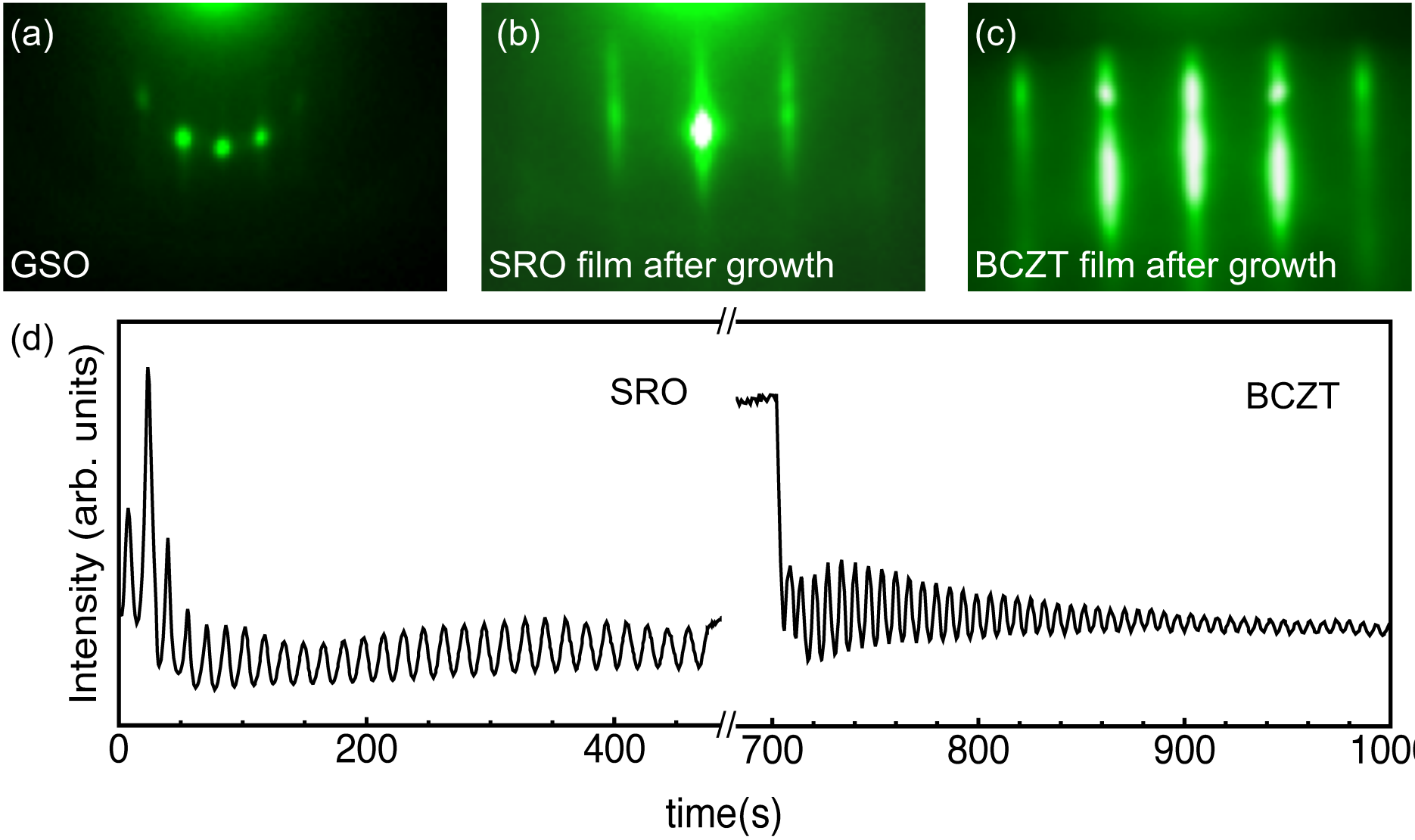
(a)
GSO
(b)
SRO film after growth
(c)
BCZT film after growth
(d)
Intensity (arb. units)
SRO
BCZT
0
200
400
700
800
900
1000
time(s)

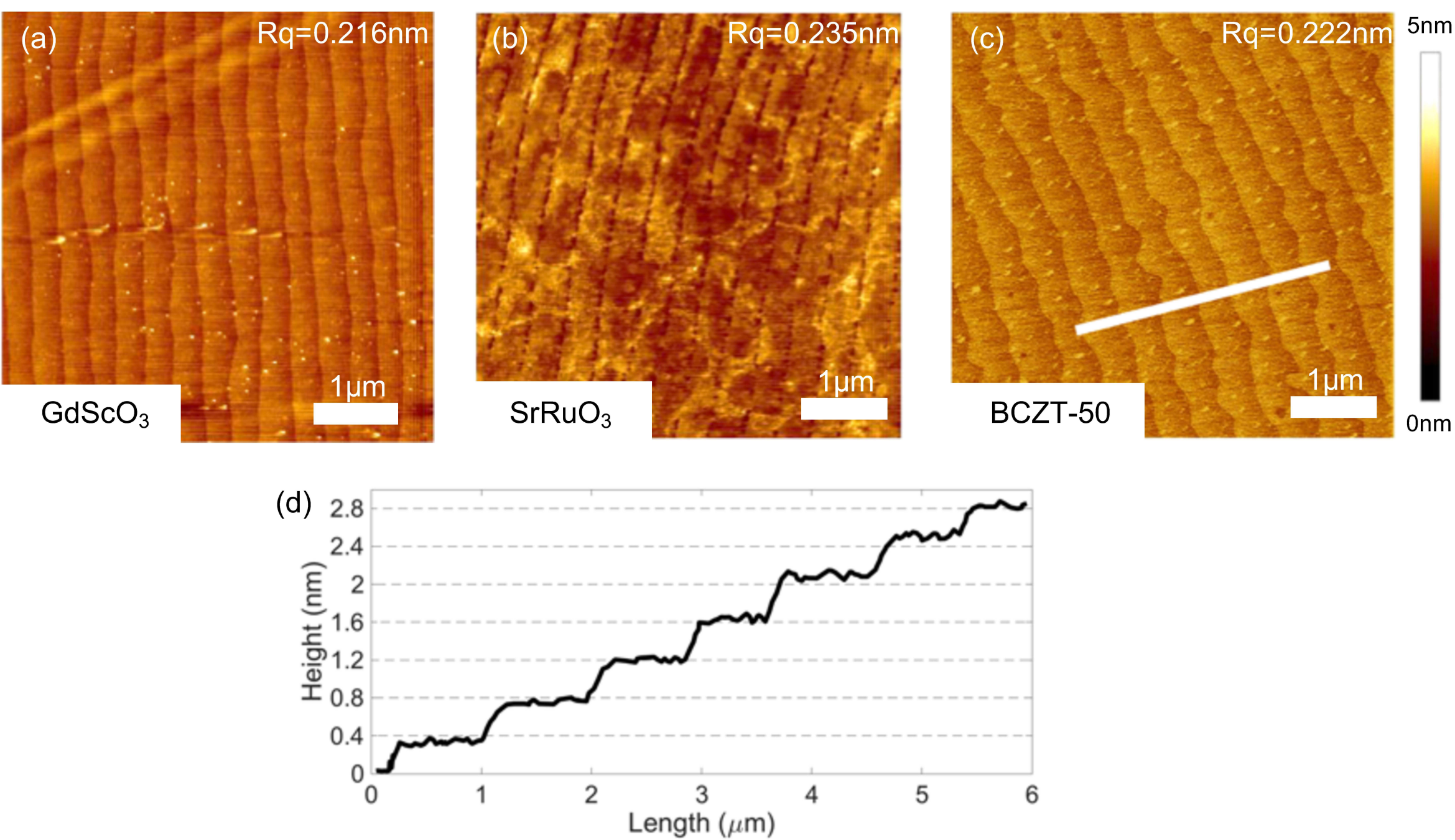
(a)
Rq=0.216nm
1μm
GdScO3
(b)
Rq=0.235nm
1μm
SrRuO3
(c)
Rq=0.222nm
1μm
BCZT-50
5nm
0nm
(d)
Height (nm)
2.8
2.4
2
1.6
1.2
0.8
0.4
0
0
1
2
3
4
5
6
Length (μm)

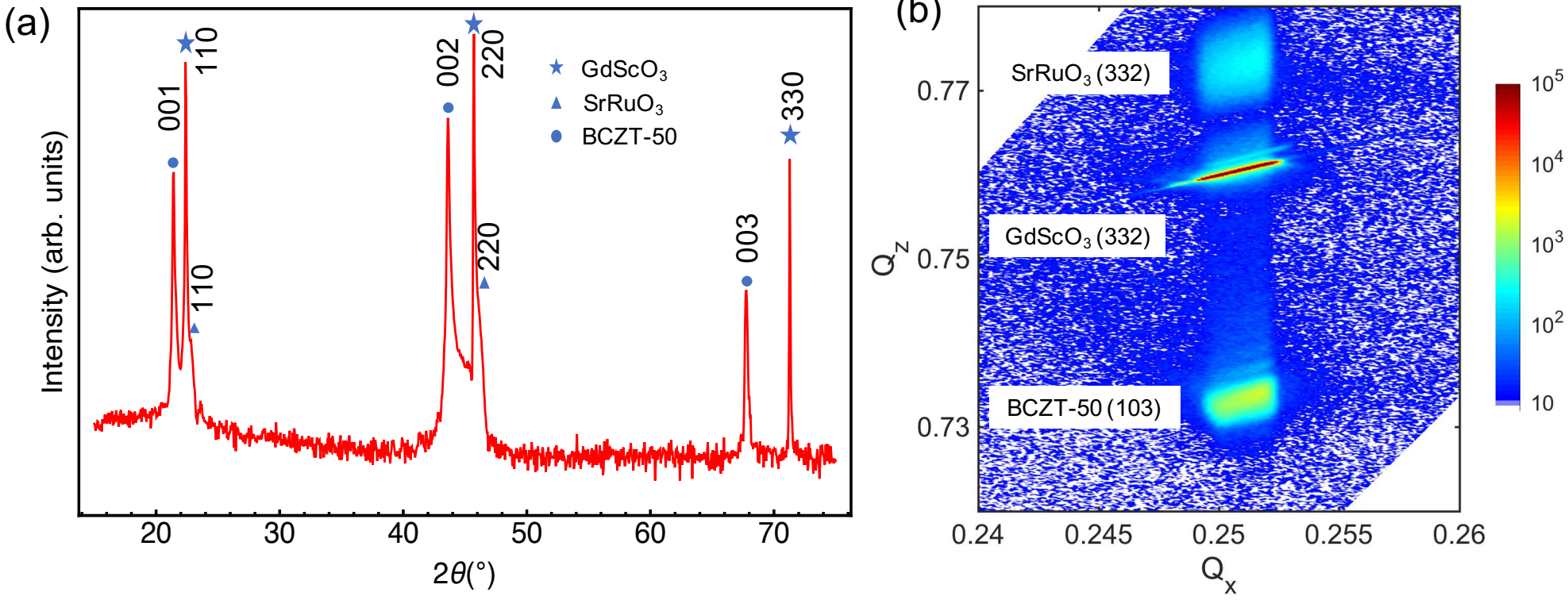
(a)
Intensity (arb. units)
2θ(°)
20
30
40
50
60
70
001
110
110
002
220
220
003
330
GdScO3
SrRuO3
BCZT-50
(b)
SrRuO3 (332)
GdScO3 (332)
BCZT-50 (103)
Qz
Qx
0.77
0.75
0.73
0.24
0.245
0.25
0.255
0.26
10^5
10^4
10^3
10^2
10

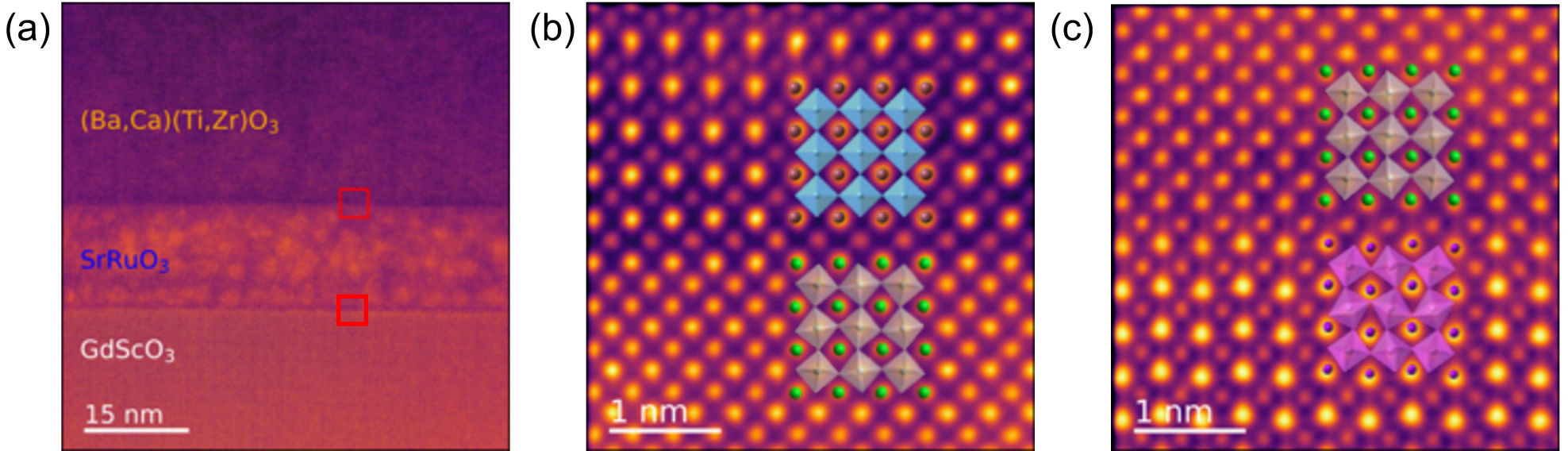
(a)
(Ba,Ca)(Ti,Zr)O3
SrRuO3
GdScO3
15 nm
(b)
1 nm
(c)
1 nm

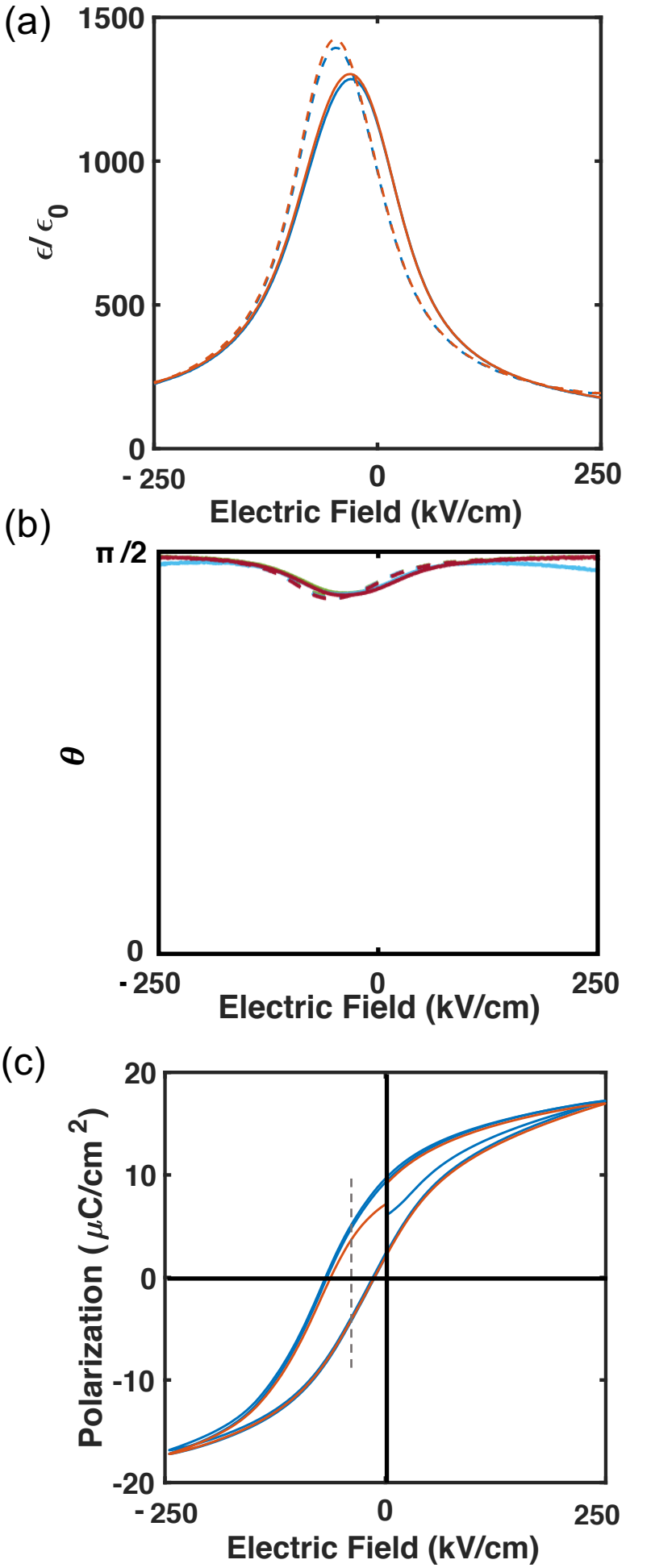
(a)
1500
1000
500
0
ϵ/ϵ_0
- 250
0
250
Electric Field (kV/cm)
(b)
π /2
0
θ
- 250
0
250
Electric Field (kV/cm)
(c)
20
10
0
-10
-20
Polarization (μC/cm^2)
- 250
0
250
Electric Field (kV/cm)